JACS
JOURNAL OF THE AMERICAN CHEMICAL SOCIETY
Article
pubs.acs.org/JACS

Direct Observation of the Formation of Surfactant Micelles under Nonisothermal Conditions by Synchrotron SAXS

Grethe Vestergaard Jensen,[*,†,⊥] Reidar Lund,[‡,#] Jérémie Gummel,[§] Michael Monkenbusch,[∥] Theyencheri Narayanan,[§] and Jan Skov Pedersen[†]

[†]Department of Chemistry and Interdisciplinary Nanoscience Center (iNANO), Aarhus University, Gustav Wieds Vej 14, DK-8000 Aarhus C, Denmark

[‡]Donostia International Physics Center, Paseo Manuel de Ladizabal 4, 20018 Donostía-San Sebastián, Spain

[§]European Synchrotron Radiation Facility (ESRF), 6 rue Jules Horowitz, F-38043 Grenoble Cedex, France

[∥]Jülich Centre for Neutron Science (JCNS) and Institute for Complex Systems (ICS), Forschungszentrum Jülich GmbH, 52425 Jülich, Germany

Supporting Information

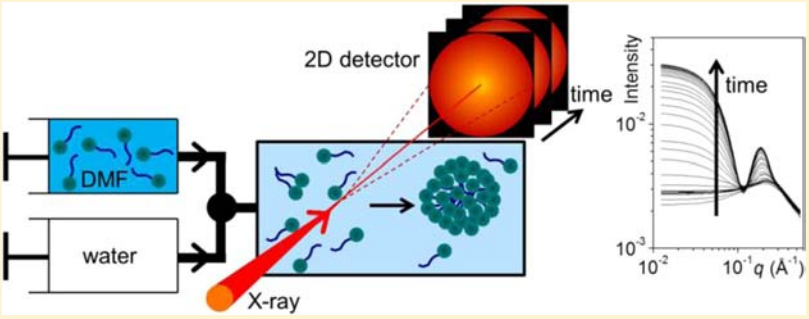

ABSTRACT: Self-assembly of amphiphilic molecules into micelles occurs on very short times scales of typically some milliseconds, and the structural evolution is therefore very challenging to observe experimentally. While rate constants of surfactant micelle kinetics have been accessed by spectroscopic techniques for decades, so far no experiments providing detailed information on the structural evolution of surfactant micelles during their formation process have been reported. In this work we show that by applying synchrotron small-angle X-ray scattering (SAXS) in combination with the stopped-flow mixing technique, the entire micelle formation process from single surfactants to equilibrium micelles can be followed in situ. Using a sugar-based surfactant system of dodecyl maltoside (DDM) in dimethylformamide (DMF), micelle formation can be induced simply by adding water, and this can be followed in situ by SAXS. Mixing of water and DMF is an exothermic process where the micelle formation process occurs under nonisothermal conditions with a temperature gradient relaxing from about 40 to 20 °C. A kinetic nucleation and growth mechanism model describing micelle formation by insertion/expulsion of single molecules under nonisothermal conditions was developed and shown to describe the data very well.

INTRODUCTION

Surfactants are ubiquitous in consumer products as important ingredients, such as detergents, solubilizers, emulsifiers, rheology modifiers, surface grafting agents, etc.[1−7] Their ability to self-assemble into a wide range of morphologies, depending on surfactant type, solvent, temperature, pH, and concentration,[8] makes them an attractive choice for the bottom-up approach of engineering nanostructured and responsive materials. This has led to new applications of surfactant systems in nanomedicine and biotechnologies, e.g., vehicles for drug delivery,[9−11] as well as templates for nanostructure fabrication.[12,13]

Equilibrium micelle structures have been widely studied over the last decades with numerous examples in the literature.[9,14−23] For this purpose small-angle scattering is very valuable as it probes the length scales that are relevant for surfactant micelles and provides structural information on the overall micelle shape and size as well as the cross-sectional (radial) micelle profile.[24] While equilibrium structures are well-studied, only relatively few studies concern the transient structures during transitions between different micellar morphologies. Such transitions occur since surfactant micelles are not static structures, but soft, dynamic systems that rearrange in response to changes in the environment. This aspect is particularly exploited in the technological applications of surfactant systems.[25,26] In order to understand and utilize these systems efficiently, it is thus highly important to obtain a more fundamental insight into the underlying mechanisms of their self-assembly properties. This is a general subject in soft

Received: December 21, 2012
Published: April 16, 2013

   dx.doi.org/10.1021/ja312469n | J. Am. Chem. Soc. 2013, 135, 7214−7222

matter science as self-assembly is at the origin of many fascinating features of amphiphilic systems. For surfactant systems, the basics of micellar kinetics have been discussed for decades, and this work brings in new insight by presenting direct structural information over the relevant size and time scales. By designing a model system, the self-assembly process could be initiated in a very controlled and reproducible manner. Using time-resolved small-angle X-ray scattering (SAXS), the structural evolution during the entire kinetic process of micelle formation from a solution of surfactant unimers was probed down to the millisecond range. Such structural kinetics, covering the entire micellization event, is crucial to understand the underlying mechanism and has not previously been reported. The results are interpreted based on a classical theory for equilibration of surfactant systems which was shown to account for the entire time evolution during micelle formation.

In general, the details of kinetic processes in micellar systems are extremely challenging to follow experimentally. Already from the 1960s and in the following decades, various methods including shock tube,[27,28] temperature jump,[27−33] and pressure jump[27,28,34−36] experiments were developed to follow micellar formation/dissociation kinetics after small perturbations of the system. Nevertheless, it was not possible to study the entire micelle formation process using these techniques. Larger perturbations were obtained using mixing experiments (junction flow[37] or stopped-flow[32]), leading to results on micelle dissolution. In all these experiments, the relaxation processes were followed by light absorption,[27−29,32] light scattering,[30] fluorescence,[28,33] and conductivity measurements.[27,28,34−36] Thus, the structural information content in the data is relatively low, and the main outcome is the estimation of relaxation times. While the experiments established that micelle formation kinetics typically occurs on a millisecond time scale, not much mechanistic insight was gained about the corresponding structural pathways. Also in more recent studies, significant attention was given to kinetic processes in micelle solutions, mainly applying larger perturbations leading to morphological changes of the structures, i.e., from globular micelles to rods by mixing with salt solutions,[38,39] from globular micelles to vesicles by a temperature jump,[40,41] or micelle dissolution by stopped-flow dilution.[42] Light scattering at a fixed angle[39−41] or fluorescence[38] were used as probes, again giving only limited structural information.

Different theoretical approaches have been followed in order to describe and explain the processes of micelle formation and equilibration.[31,43−51] An early, classic theory by Aniansson and Wall[43,44] described the equilibration after small perturbations from equilibrium, assuming that only the event of insertion or expulsion of single surfactant molecules to/from a micelle contributes. Kahlweit included in addition the mechanism of fusion or fission of micelles to explain observations made for the long relaxation times.[45] The theoretical predictions for the dependencies of the relaxation times on surfactant concentration have been tested against experimentally obtained relaxation times.[28] In order to obtain more conclusive insight into the kinetics and its pathways, the structural evolution should be investigated simultaneously; something that cannot be achieved with the applied classical methods.

With the development of high-brilliance X-ray beamlines at third-generation synchrotron radiation sources and of advanced instrumentation, time-resolved SAXS has become possible with a temporal resolution in the millisecond time range and even below.[52] This, in addition to the structural resolution of SAXS, makes this technique very powerful for studying kinetic processes in surfactant solutions.[53,54] Employing this technique, detailed structural information on the shape, size, and aggregation number of the micelles can be determined in situ during the equilibration process. So far, synchrotron SAXS has been applied in combination with stopped-flow mixing for several studies of surfactant vesicle formation[55−62] and in one case for investigating block copolymer micelle formation.[46] Direct observation of micelle formation processes of surfactant systems, however, is to our knowledge so far lacking.

Here we show that it is possible to obtain complete real-time structural information on the micelle structures during the entire course of surfactant micelle formation by combining stopped-flow mixing and synchrotron SAXS to and probe this key fundamental process. This is done by mixing singly dissolved dodecyl maltoside (DDM) surfactant molecules ('unimers') in dimethyl formamide (DMF) with water, which results in a lower solubility of the surfactant and hence induces micelle formation. A similar approach was used to investigate block copolymer micelles.[46] Here we show that it is possible to follow the process even for small surfactant molecules for a relatively wide range of surfactant concentrations. Mixing water and DMF is an exothermic process, causing the equilibration process to take place under nonisothermal conditions mimicking classical temperature jump experiments. However, in contrast to earlier experiments, a complete structural resolution is provided during the kinetic process. We show that by employing a nucleation and growth model and allowing for a time-dependent system temperature during the micelle formation process, the results can be understood quantitatively. This gives considerable fundamental insight into the mechanism of self-assembly that most certainly will pave the way for more quantitative design of surfactant systems in future applications. The work also serves to demonstrate the general potential of the combination of synchrotron SAXS and stopped-flow mixing for studying kinetic processes in soft matter and other physicochemical systems on the millisecond scale. In particular, the data analysis using advanced scattering models as well as kinetic nucleation and growth models is pertinent to a wide range of physicochemical problems and is likely to inspire similar works in other fields.

EXPERIMENTAL SECTION

Materials. Dodecyl-β-D-maltoside (dodecyl maltoside, DDM) was purchased from Glycon Biochemicals GmbH (>99.5%). *N*,*N*-Dimethylformamide (DMF) was purchased from Sigma Aldrich. Both DDM and DMF were used as received.

Determination of the Critical Micelle Concentration. The critical micelle concentration (cmc) of DDM in 50 vol% DMF was determined by surface tension measurements, dynamic light scattering (DLS) measurements, and static SAXS measurements of solutions at different DDM concentrations in the range from 0.1 to 2 wt %. A cmc of 0.65 wt % was determined from the surface tension measurements and confirmed by both DLS and SAXS. The results are presented in the Supporting Information (SI).

Synchrotron SAXS. The time-resolved SAXS measurements were performed at the ID02 beamline at the European Synchrotron Radiation Facility (ESRF) in Grenoble.[54] This undulator beamline provides intensities which allowed for collection of high-quality data with acquisition times of 2−10 ms. We found that 10 ms exposure time was enough to ensure good statistics but at the same time minimize radiation damage effects with higher flux (10^{14} photons/s). The two-dimensional time-resolved SAXS patterns were recorded

using a fast read-out, low-noise CCD detector (FReLoN). The incident X-ray wavelength λ was 0.995 Å, and the sample−detector distance was 1 m, giving a range of the modulus, q, of the scattering vector of 0.01−0.6 Å^{-1}, where $q = 4\pi \sin(\theta)/\lambda$ and 2θ is the scattering angle. A BioLogic SFM-400 stopped-flow device was used for rapid mixing of water and DDM/DMF solutions.[54] Experiments were performed for DDM concentrations in DMF of approximately 1.5, 1.8, 2, 2.6, and 3 wt %. For each mixing experiment, 200 μL of DDM solution was mixed with an equal volume of water. After mixing, the solution was transferred to the measurement capillary with a dead time of ∼2.5 ms, and this set the earliest kinetic time for which data can be collected. The detector read-out time was $t_{\text{read-out}}$ = 190 ms for the 4 × 4 pixel binning, and the low noise readout mode used. To avoid oversampling, the time between each consecutive measurement, t_{dead}, was increased in a geometric progression with each data frame i according to $t_{\text{dead},i} = t_{\text{read-out}} g^{i-1}$, with g = 1.11. The solvent scattering was measured by mixing water and DMF using the stopped-flow apparatus in the same way as for the kinetic experiments. As this mixing is exothermic, the temperature was not constant with time but rather equilibrated with time from higher temperature obtained upon mixing.

Temperature Profile during Mixing of DMF and Water. The temporal evolution of the temperature after mixing a solution in DMF with water was determined by collecting time-resolved scattering patterns after mixing pure DMF and water 1:1. The sample temperature can be written as $T = T_\infty + \Delta T$, where T_∞ is the temperature at equilibrium (room temperature). For a homogeneous liquid mixture, the scattered intensity, I, at low q scales with absolute temperature, the square of the density, and the osmotic compressibility of the mixture. Since density and compressibility only have a weak temperature dependence in the relevant temperature interval,[63,64] ΔT can be determined according to the equation $\Delta T/T_\infty = (I - I_\infty)/I_\infty$. I was taken as the average intensity in the q range from 0.05 to 0.13 Å^{-1}, where the scattering is nearly flat and well-defined. ΔT is plotted against time after mixing, t, in Figure 1. The full line is a fit to an offset exponential decay, giving decay time of $\tau_{\text{d,exp}}$ = 7.8 ± 0.4 s.

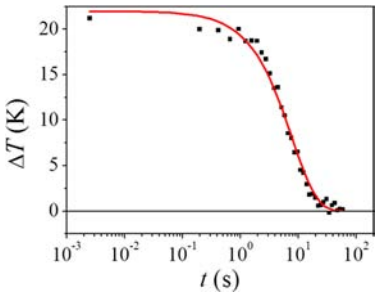

Figure 1. Temporal evolution of the sample temperature, calculated from the average scattered intensity in the interval q = 0.05 to 0.13 Å^{-1}, after mixing of DMF and water 1:1 by volume.

Temperature Dependence of Solvent Viscosity. The viscosity of a 1:1 water−DMF mixture was measured in the relevant temperature interval. The results are shown in the SI. An Arrhenius function was fitted to the data, giving the temperature dependence: $\eta(T) = \eta_0 + A \exp(-T/T')$, with η_0 = (0.753 ± 0.007) mPa s, A = 4.69 ± 0.01, and T' = (21.9 ± 0.1) °C.

Solution Densities and Determination of Specific Volumes. The contrasts for the DDM head and tail group were determined from measurements of specific volumes, V_{surf}, for DDM at 25 °C using an Anton Paar DM 5000 densimeter. A literature value of V_{tail} = 352.4 Å^3 for the specific volume of the C_{12} tail was used.[65] The volume of the headgroup was $V_{\text{head}} = V_{\text{surf}} - V_{\text{tail}}$ = 353.7 Å^3, using this value for the tail. The temperature was not constant during a kinetic experiment, which led to a slight change of the specific volume of DDM. However, the contrast of DDM in a 1:1 water−DMF solvent changed only marginally with temperature, as the density of the solvent also decreased with temperature (see SI). Furthermore, it is very difficult to quantify the change in contrast for the headgroup and the tail separately, as this required a value for the specific volume of the tail as a function of temperature, which to our knowledge is not available. Thus, the same contrasts were applied for all temperatures.

MODEL THEORY

Structural Model. All the SAXS data were fitted on absolute scale by a structural model consisting of contributions from oblate micelles and singly dissolved surfactants. A schematic drawing of the model is shown in Figure 2. The

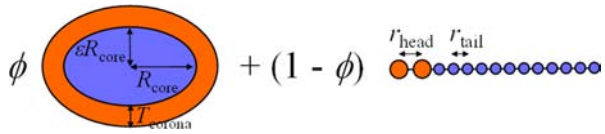

Figure 2. Structural model fitted to the SAXS data. A fraction ϕ of the surfactant molecules is aggregated into ellipsoidal micelles with core radii R_{core} and $\varepsilon R_{\text{core}}$ and a corona thickness T_{corona}. The remaining molecules are singly dissolved and modeled by points on a line (see text).

characteristic scattering from the singly dissolved surfactants can be observed in the first data frames for the experiment at the lowest investigated DDM concentration of 0.77 wt %. The oscillation in the scattering data stems from the interference in the scattering from the hydrocarbon tail, which has a negative contrast, and the maltoside headgroup, which has a positive contrast. To describe this characteristic pattern, an expression is suggested, in which the scattering pattern is parametrized by the scattering from a linear array of 14 scattering points, which serves as a rough model for the individual surfactant molecules. Whereas an actual molecule is expected to have a variety of conformations, this model reflects the limited spatial resolution of SAXS and is able to account for all features in the observed scattering patterns. The excess scattering length of the headgroup is associated with 2 points at one end, and the excess scattering length of the tail with the remaining 12 points. The scattering from the surfactant model can be obtained as a sum over the interference contributions from each of the point pairs, where i and j denote the points:

$$P_{\text{surf}}(q) = \sum_{i,j} \Delta\rho_i \Delta\rho_j V_i V_j \frac{\sin(qr_{ij})}{qr_{ij}} \quad (1)$$

V_i is the volume associated with point i. Thus, for a point in the headgroup, $V_i = V_{\text{head1}}/2$, and for a point in the tail, $V_i = V_{\text{tail1}}/12$, where V_{head1} and V_{tail1} are, respectively, the specific volume of the maltoside headgroup and the C_{12} tail of the singly dissolved surfactant. V_{head1} and V_{tail1} were taken as fit parameters since one cannot expect them to be identical to those determined by densimetry (see above) at higher concentration where the micellar state is predominant, and since the model does not describe the actual structure of the molecule exactly. Their values determine the scattering length density of the head and the tail, ρ_{head1} and ρ_{tail1}, respectively. $\Delta\rho_i$ is the excess scattering length density of point i with respect to the solvent (and is thus equal to the contrast of either the headgroup or the tail, $\Delta\rho_{\text{head1}}$ or $\Delta\rho_{\text{tail1}}$), and r_{ij} is the distance between point i and j. The data were fitted by a model using the distance between the two headgroup points, r_{head}, as a fit parameter. As the length of a stretched C_{12} chain is 16.7 Å,

dx.doi.org/10.1021/ja312469n | J. Am. Chem. Soc. 2013, 135, 7214−7222

the distance between the points associated with the tail was fixed at (16.7 Å)/12.

The micelles are modeled as ellipsoidal core−corona particles with a core of radius R_{core}, an aspect ratio ε, and a corona of thickness T_{corona} formed by the maltoside head groups. Thus, the total micelle radius is $R_{tot} = R_{core} + T_{corona}$. As the corona thickness should be the same along each ellipsoid axis, the aspect ratio of the total micelle is $\varepsilon_{tot} = (\varepsilon R_{core} + T_{corona})/(R_{core} + T_{corona})$. The scattering amplitude from a sphere of radius R is given by $\Phi(qR) = 3[\sin(qR) - qR\cos(qR)]/(qR)^3$. Then, the scattering form factor for the ellipsoidal micelles is given by[66]

$$P_{mic}(q) = \int_0^{\pi/2} [\Delta\rho_{corona} V_{tot} \Phi(qR'_{tot}) + (\Delta\rho_{core} - \Delta\rho_{corona}) V_{core} \Phi(qR'_{core})]^2 \sin\alpha d\alpha \quad (2)$$

where $R'_{core} = R_{core}(\sin^2\alpha + \varepsilon^2\cos^2\alpha)^{1/2}$ and $R'_{tot} = R_{tot}(\sin^2\alpha + \varepsilon_{tot}^2\cos^2\alpha)^{1/2}$. V_{tot} and V_{core} are the volumes of the total micelle and the core, respectively: $V_{core} = (4/3)\pi R_{core}^3\varepsilon$, and $V_{tot} = (4/3)\pi R_{tot}^3\varepsilon_{tot}$. The excess scattering length densities (contrasts) $\Delta\rho$ were determined from the specific volumes for the DDM head and tail group (see Experimental section), V_{head} and V_{tail}, as $\Delta\rho_{head} = Z_{head}/V_{head}$ and $\Delta\rho_{tail} = Z_{tail}/V_{tail}$, where Z_{head} and Z_{tail} are the number of electrons in the surfactant head and tail group, respectively. For all fits presented here, it was assumed that the micelle cores are dry, giving $\Delta\rho_{core} = \Delta\rho_{tail}$. The corona contains solvent, and the contrast of the corona is given by $\Delta\rho_{corona} = \Delta\rho_{head}(V_{tot} - V_{core})/(p_{mic}V_{head})$.

The total scattering from the surfactant solution is described by the model:

$$I(q) = \frac{N}{V}\left[\frac{\varphi}{p_{mic}} P_{mic}(q) + (1 - \varphi) P_{surf}(q)\right] \quad (3)$$

where N/V is the total number concentration of surfactant molecules, and ϕ is the fraction of surfactant molecules in the micelles. A constant to describe any residual flat background was also added to the model when performing the fits to the data.

Kinetic Model. Following the approach by Lund et al.,[46] which is based on the model by Neu et al.,[47] it is assumed that only single insertion/expulsion steps dominates the growth of the micelle (see Figure 3). With this assumption the flux for creation of micelles of aggregation number $p + 1$ can be written as

$$j_{p+1} = k_{+,p}\phi_1\phi_p - k_{-,p+1}\phi_{p+1} \quad (4)$$

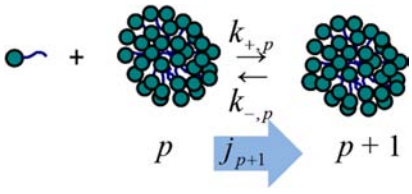

Figure 3. Mechanism for micelle formation by stepwise insertion/expulsion of single surfactant molecules into a micelle of aggregation number p resulting in an aggregation number $p + 1$. This mechanism results in a flux j_{p+1} from micelles of aggregation number p to micelles of aggregation number $p + 1$.

where φ_p is the volume fraction of aggregates of aggregation number p, and $k_{+,p}$ and $k_{-,p+1}$ are the rate constants for the insertion and expulsion, respectively. Applying the detailed balance condition giving that $k_{+,p}\varphi_1\varphi_p = k_{-,p+1}\varphi_{p+1}$, the following expression is obtained[47]

$$j_{p+1} = k_{+,p}\phi_1[\phi_p - \phi_{p+1}\exp(G(p+1,\phi_1) - G(p,\phi_1))] \quad (5)$$

Here it is used that $\varphi_p = \exp[-G(p,\varphi_1)]$, where $G(p,\varphi_1)$ is the potential (in units of k_BT where k_B is Boltzmann's constant and T is the absolute temperature) of formation of a micelle of aggregation number p at a volume fraction φ_1 of singly dissolved surfactants in the solution.

The potential $G(p,\varphi_1)$ can be written as[48]

$$G(p,\phi_1) = F_{mic}(p) - pF_1 - (p-1)\ln(\phi_1/c_{sca}) \quad (6)$$

where $F_{mic}(p)$ is the free energy (in units of k_BT) of a micelle of aggregation number p. F_1 is the free energy for a singly dissolved surfactant molecule. It is here approximated by $F_1 = F_{mic}(1)$. The third term gives the loss of mixing entropy associated with the micelle formation. Only roughly estimated, c_{sca} is a correction term for the potential, which can be expected as the free energy of a unimer. This correction also includes a reference entropy term for the unimer. The correction factor is introduced in a way so that it does not change the functional form of $G(p)$, which still has minima at $p = 1$ and $p = p_{eq}$.

The following expression is applied for the micelle free energy:

$$F_{mic}(p) = \gamma' p^{2/3} + \beta p^{5/3} \quad (7)$$

The first term gives the surface free energy of the micelle core, and γ' is the reduced surface tension. For a spherical micelle core of radius R_{core} consisting of surfactant tails of volume V_{C12} with a surface tension γ toward the solvent, the surface free energy equals $\gamma 4\pi R_{core}^2/k_BT = \gamma 4\pi\,(3pV_{C12}/(4\pi))^{2/3}/k_BT = \gamma\,(36\pi V_{C12}^2)^{1/3}p^{2/3}/k_BT$. Thus, the reduced surface tension is $\gamma' = \gamma\,(36\pi V_{C12}^2)^{1/3}/k_BT$. The second term in eq 7 assures that the energy per surfactant molecule, $F_{mic}(p)/p$, increases at high p. Lund et al.[46] applied a scaling $\sim p^{3/2}$, which can be assumed for a polymeric surfactant headgroup.[67] The scaling $\sim p^{5/3}$ applied here approximates the energy increase when stretching the surfactant tails to accommodate for the larger micelle cores with increasing p.[68]

The flux given in eq 5 can be calculated for each p from the parameters entering $G(p,\varphi_1)$ and the rate constant $k_{+,p}$. If the rate of insertion of a unimer into a micelle of aggregation number p is limited by the diffusion of the unimeric surfactant molecules and the micelles, $k_{+,p}$ (in units of cm^3/s) can be written as[69]

$$k_{+,p} = 4\pi R_{coll}(D_{app,1} + D_{app,p}) \quad (8)$$

The micelle collision radius, R_{coll} can be given as the sum of the radii of the unimer, R_1, and of the micelle, R_p, $R_{coll} = R_1 + R_p$. $R_p = (3pV_{surf}/(4\pi))^{1/3}$, where V_{surf} is the volume of a surfactant molecule. For R_1, the same expression is applied, with $p = 1$. $D_{app,p}$ is the apparent diffusion constant of a micelle of aggregation number p (for $D_{app,1}$, $p = 1$). It is given by the Stokes−Einstein equation as $D_{app,p} = k_BT/(6\pi\eta R_p)$. Thus, the rate constant can be written as a function of p and the temperature-dependent solvent viscosity, $\eta(T)$:[70]

dx.doi.org/10.1021/ja312469n | J. Am. Chem. Soc. 2013, 135, 7214−7222

$$k_{+,p} = x\frac{2k_BT}{3\eta(T)}\frac{(1+p^{1/3})^2}{p^{1/3}} \quad (9)$$

where x is a prefactor, which can account for further (p, T, and η independent) kinetic barriers for the micelle growth, and $\eta(T)$ was determined experimentally (see the Experimental section). The entire equilibration of the system from surfactant unimers to the final micelle solution is given by the set of differential equations:

$$\frac{d\phi_p}{dt} = j_p - j_{p+1} \quad (10)$$

The temporal evolution of the distribution of aggregation numbers can be determined by solving this set of equations simultaneously for a set of the four input parameters c_{sca}, γ', β, and x. In the present study, these four parameters were used as fit parameters to obtain the best possible fit to an experimentally determined temporal evolution of the weight-average aggregation number of the micelles. Note that γ' scales with T^{-1}, which means that the nonisothermal nature of the process is included through γ' as well as through the expression for $k_{+,p}$ in eq 9.

RESULTS AND DISCUSSION

Three examples of time-resolved series of scattering data showing in situ observation of formation of micelles after adding water to DDM/DMF solutions are depicted in Figure 4a,c,e. The remaining SAXS data sets are shown in the SI.

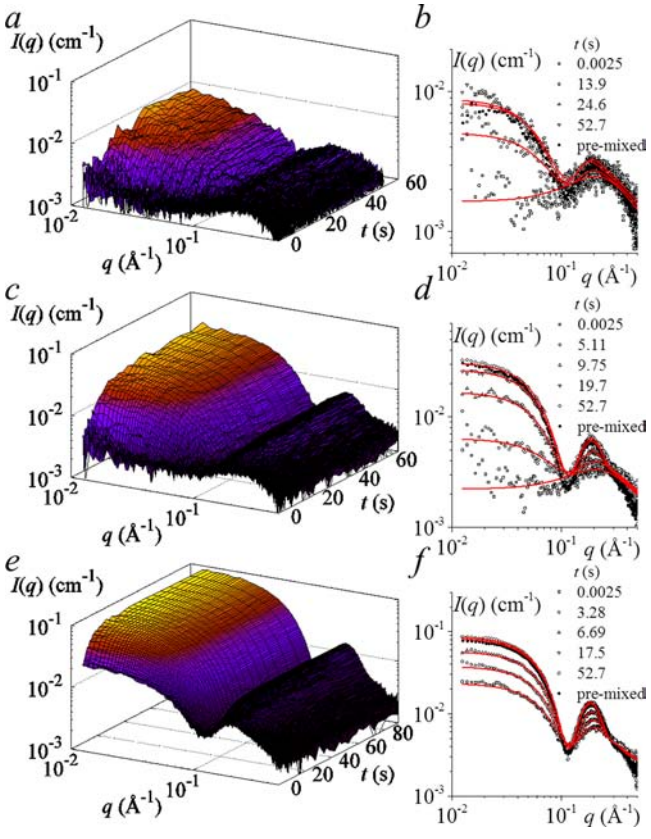

Figure 4. (a,c,e) SAXS data collected at times t after mixing water and a DDM solution in DMF for a final DDM concentration of 0.77, 1.0, and 1.5 wt %, respectively. (b,d,f) Representative data plots with model fits (full lines) are shown.

For the first few frames for the lowest concentration, the scattering pattern is very flat, and only a small oscillation at high q is visible showing that the data corresponds to singly dissolved DDM molecules. With time, the contribution, characteristic for the scattering from micelles, increases. Thus, the entire kinetic process from a solution of singly dissolved surfactants to the final equilibrium micelle solution is covered by the experiment.

Fit of Structural Model. To obtain more detailed information on the structural evolution, the structural model given in eq 3 was fitted to the entire data set on absolute scale. Examples of the model fits to data are shown in Figure 4b,d,f for DDM concentrations of 0.77, 1.0, and 1.5 wt %, respectively. Data and model fits for static SAXS measurements of equilibrium mixtures (both below and above the cmc) are given in the SI. The fit parameters for the singly dissolved surfactants were fixed at values obtained by a fit of the expression in eq 1 to the initial frame of the experiment at the lowest DDM concentration. The fit gave values V_{head1} = 333 ± 2 Å^3, V_{tail1} = 341 ± 1 Å^3, and r_{head} = 6.7 ± 0.2 Å, which are reasonable compared to the physical dimensions of a DDM molecule, especially taking the simplified model representation of the molecule into account.

In order to increase the stability of the fits, the thickness of the micelle corona was fixed at a value of 10 Å in all cases. This corresponds to the value obtained after simultaneous fitting data for three concentrations of the micelles at equilibrium. The value corresponds well with the expected size of the maltoside headgroup, which should not change significantly during the course of the kinetic process. The parameters resulting from the fits are plotted in Figure 5. Panel a shows the evolution of the fraction of surfactant molecules in micelles, ϕ. The equilibrium values of ϕ confirm the same concentration of singly dissolved surfactants, which equals cmc = $(1 - \phi)c$. The slope of the straight line fit in the plot in Figure 5b of $(1 - \phi)$ against c should thus correspond to cmc. The obtained value of 0.66 wt %, agrees well with the experimentally determined value for cmc (see SI).

The micelle core radii, R_{core} and εR_{core}, only show a slight growth with time t. In the two long directions, R_{core} increases from about 18 to 19 Å, whereas in the short direction εR_{core} increases from around 9 to 11 Å, corresponding to an increase in aggregation number from about 35 to 47. Thus, no evidence of very small premicellar aggregates is found. The best fits are obtained for aspect ratio of the core, ε, smaller than unity, suggesting that the micelles are oblate rather than prolate. The slightly more pronounced increase in εR_{core} with time indicates that the micelles become less aniosotropic (less flattened oblates) during the relaxation. It should be noted that only slightly poorer fits are obtained for a model of prolate ellipsoidal micelles ($\varepsilon > 1$), and it is thus not possible from the time-resolved SAXS data alone to determine with certainty which of these two morphologies are dominant. However, surfactant systems are very dynamic, and it is likely that, due to shape fluctuations, both are present. It should be noted that this choice of oblate micelles over prolate for the structural model does not change the main conclusions of this study.

Polydispersity is not included in the model fits, as the fit quality is high for the monodisperse model, meaning that an additional fit parameter need not be introduced. Furthermore, a parameter giving the width of a size distribution would couple strongly with the aspect ratio parameter, ε. The only option would be to include polydispersity instead of ellipticity and

dx.doi.org/10.1021/ja312469n | J. Am. Chem. Soc. 2013, 135, 7214−7222

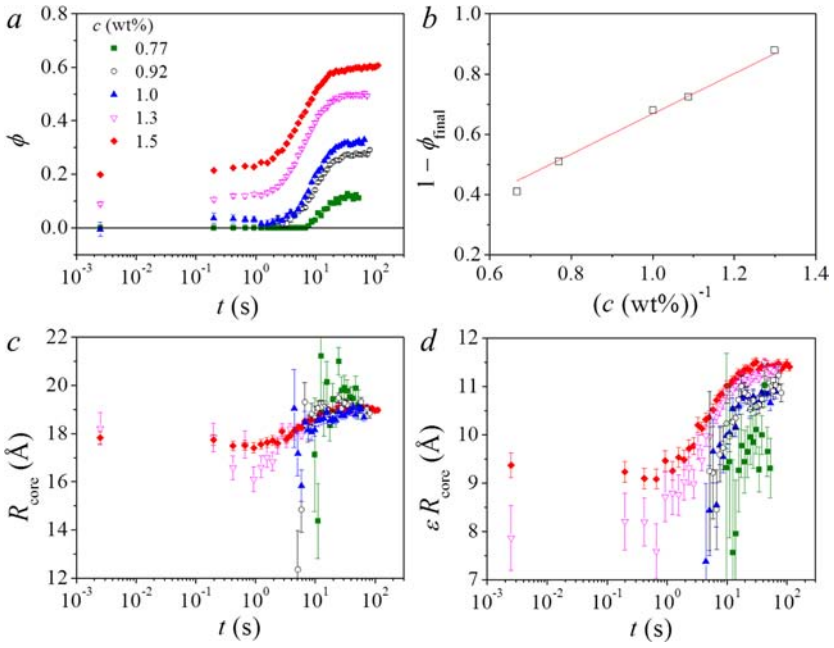

Figure 5. Parameters resulting from the fit of the structural model to the data frames recorded at times t after mixing DDM solutions in DMF with water 1:1 by volume for DDM concentrations of 0.77 (green squares), 0.92 (black circles), 1.0 (blue upward triangles), 1.3 (magenta downward triangles), and 1.5 (red diamonds) wt%. (a) Fraction of surfactant molecules in micelles. (b) The final fraction of surfactant molecules in micelles, ϕ_{final} plotted as $1 - \phi_{final}$ against the surfactant concentration. The line is a linear fit, where the slope is expected to be equal to cmc (see text). (c) Core radius of the ellipsoidal micelles in the two long directions. (d) Core radius of micelles in the short direction.

hence use a model of polydisperse spheres. However, as the data clearly show that core dimensions exceeding the length of a stretched surfactant tail are represented in the sample, and therefore the distribution of the sphere radii would need to include these dimensions. This is not physically realistic for the surfactant molecules, and hence this model was excluded.

Fit of Kinetic Model. To obtain a detailed understanding of the mechanisms underlying the kinetic evolution of the system, it is necessary to compare the results to a mechanistic kinetic model. The kinetic model, which was described above, describes the aggregation process by a mechanism where only insertion/expulsion of single unimers to the micelles contributes. The model gives the total expected temporal evolution of the size distribution of micelles for a set of system parameters c_{sca}, γ', β, and x, as described in the section on the kinetic model. To test the kinetic model against the SAXS data, these parameters must be optimized to obtain the best possible fit to the experimental results. Here we fit the kinetic model to the weight-average aggregation number, p_w, which can be obtained from the scattering intensity at $q = 0$, $I(q = 0)$, without making any structural assumptions for the scattering objects (see SI for details). The resulting values are plotted in Figure 6.

As the temperature was not constant during the experiment, the kinetic model had to be modified to take into account the time-dependent temperature profile. The temperature dependence is included through the reduced core surface tension, γ', which is inversely proportional to the temperature (eq 7) and through the rate constants, which depend on the temperature both directly and through the viscosity $\eta(T)$ (eq 9). The time-dependent reduced surface tension is given by $\gamma'(t) = (298\ \mathrm{K}) \times \gamma'_0/T(t)$, where γ'_0 is the reduced surface tension at $T = 298$ K and is applied as a time-independent free fit parameter. The time-dependent solvent viscosity is determined experimentally and can be described by $\eta(t) = \eta_0 + A \exp(-T(t)/T')$ with $\eta_0 = (0.753 \pm 0.007)$ mPa s, $A = 4.69 \pm 0.01$ mPa s, and $T' = (21.9 \pm 0.1)$ °C, as explained in the Experimental section. The time-dependent temperature was included as

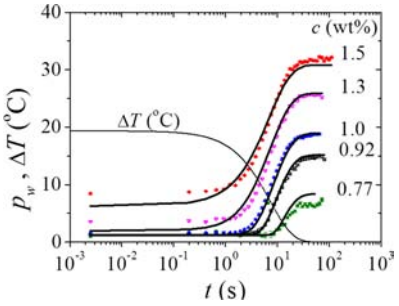

Figure 6. Weight-average aggregation numbers, p_w, of DDM at times t after mixing DDM solutions in DMF with water 1:1 by volume, obtained by model independent Guinier fits to the scattering data for $q < 0.07$ Å^{-1}. The DDM concentrations in the final solutions are 0.77 (green squares), 0.92 (black circles), 1.0 (blue upward triangles), 1.3 (magenta downward triangles), and 1.5 (red diamonds) wt%. The solid lines are simultaneous fits to the kinetic model (see Kinetic Model section). The dashed line gives the excess temperature, ΔT, used in the fit of the kinetic model.

$$T(t) = 298\mathrm{K} + \Delta T(1 - \exp(-t/\tau_i))^{4.2} \exp(-t/\tau_d) \quad (11)$$

The amplitude for the temperature increase, ΔT, the time for the increase, τ_i, and the time for the decay, τ_d, were then included as additional parameters in the fit to the kinetic model. The exponent of 4.2 in eq 11 was chosen to ensure a sufficiently steep temperature increase so that the temperature had increased to its maximum at the time corresponding to the first SAXS data frame.

The simultaneous fit of the kinetic model to p_w for all DDM concentrations is plotted in Figure 6 as the full lines. The model fits the experimental values rather well for all concentrations of

dx.doi.org/10.1021/ja312469n | J. Am. Chem. Soc. 2013, 135, 7214−7222

DDM. This supports the interpretation that the mechanism of insertion/expulsion of single unimers to the micelles is indeed the dominant mechanism for the micelle formation and growth. Other pathways cannot be completely excluded, but they seem to be of relatively low significance. The fit was obtained for a set of parameters of which some were fixed and others were optimized. The sensitivity of the fit toward the different free parameters has been tested, showing that the possible variance of each of them is <1%. The final values of fit parameters correspond to physically realistic values, which further validates the results. The time constant giving the initial temperature increase was fixed to an arbitrary value of 0.06 ms, effectively corresponding to an instantaneous increase of the temperature as the sample is mixed. The exact value should be comparable to the mixing dead time (~0.1 ms), but it is of no consequence for our results as the transfer dead time before the first SAXS acquisition is much larger (2.5 ms). The temperature decay time obtained from fitting was $\tau_d = 7.3 \pm 0.3$ s, which coincides well with the value $\tau_{d,exp} = 7.8 \pm 0.4$ s determined from a separate scattering experiment when mixing the pure solvents, water and DMF (see Experimental section). The fitted amplitude for the temperature increase, $\Delta T = 28$ °C, is reasonably close to $\Delta T = 22$ °C, that was derived from the mixing of pure water and DMF, and also to the increase of 17.6 °C observed when mixing large quantities of water and DMF (40 mL of each).

The reduced surface tension was determined to be $\gamma_0' = 10.30 \pm 0.01$, giving a surface tension for the core of 17.6 mN/m at $T = 298$ K. This value will be influenced by the type and surface density of the surfactant head groups. The value is comparable to an experimental value of 22.0 mN/m that was reported at 20 °C for the aliphatic polymer poly(ethylene-alt-propylene), which, however, has a chemical structure deviating from that of the C_{12} chain of DDM. The scale factor for the second term of eq 7 is $\beta = 0.0689 \pm 0.0001$, and c_{sca}, the correction factor, is $c_{sca} = 60.20. \pm 0.01$. In an earlier work on micelle formation of polymeric surfactants, a significantly higher correction factor of 2.8×10^5 was necessary in order to describe the data. Thus, we speculate that the correction factor is associated with the loss in entropy for a unimer due to the interconnectivity of the surfactant chain.

The prefactor for the rate constant, $k_{+,p}$ (eq 9) was determined to be $x = 4.25 \times 10^{-4}$. Since $x < 1$, it represents an additional reaction barrier (of 7.8 k_BT). As the barrier for the insertion process itself is expected to be quite small,[49] this must relate to the fact that a certain orientation of the surfactant toward the micelle, as well as an exposed area of the micelle core facing the surfactant, is needed for a successful insertion event. This interpretation was introduced by Mohan and Kopelevich, based on a simulation study of micelle formation in a different surfactant system.[49] If it is assumed that the reaction barrier only stems from the surfactant orientation (neglecting other contributions, such as enthalpic barriers or cooperative reorganization in micelles), the allowed angular deviation of the surfactant orientation toward the micelle, $\pm \theta_{orient}$, can be determined. The values x and θ_{orient} are related by $x = \Omega_{orient}/4\pi$, where Ω_{orient} is the solid angle that the allowed surfactant orientations cover, $\Omega_{orient} = 2\pi(1 - \cos(\theta_{orient}))$. The determined value for x corresponds to a value for θ_{orient} of 2.4°, indicating that the surfactant must adopt a very specific orientation for a successful incorporation into the micelle. Other effects which might contribute to the additional barrier for the process could be the necessity for the surfactants in the micelles to rearrange to make room for the incorporating molecule or the unfavorable process of pushing the hydrocarbon tail of the inserting surfactant through the headgroup shell of the micelle.

The temporal evolution of the distribution of aggregation numbers for the unimers/micelles resulting from the kinetic model is plotted in Figure 7 for the lowest and highest DDM concentrations, respectively. For the highest concentration, micelles are formed already at the first measurement time at $t = 2.5$ ms, whereas only small oligomers are present for the lowest concentration. At the time where the temperature decreases again, $t = \tau_d$, even more micelles are formed for the highest concentration, and the average micelle aggregation number increases. This is associated with a decrease in concentration of small oligomers. For the lowest DDM concentration, a small increase in the oligomer contribution is observed around $t = \tau_d$. After τ_d, the concentration of the oligomers decreases again, as micelles are formed. Plots of the time evolution of unimers and dimers are given in the SI. The smallest oligomers follow the same trends as the dimers.

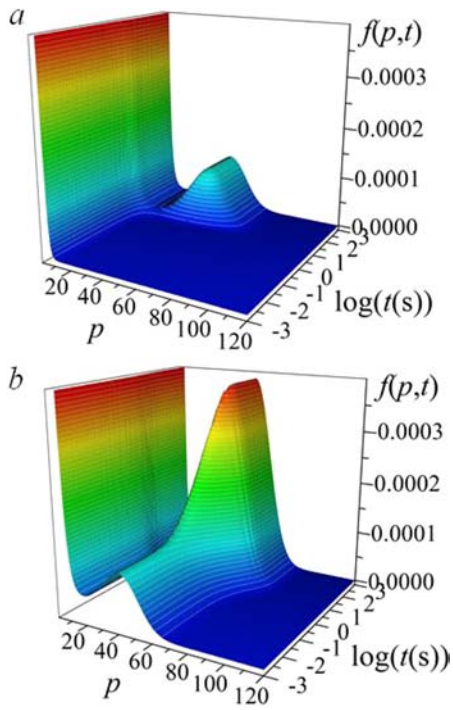

Figure 7. Temporal evolution of the distribution of aggregation numbers according to the kinetic model fitted to the experimentally determined weight-average aggregation numbers for surfactant concentrations of (a) 0.77 and (b) 1.5 wt %.

In general, the size distributions are bimodal as only unimers (and oligomers of very low aggregation numbers) and micelles of an aggregation number close to the final equilibrium micelle aggregation number contribute. This is consistent with the entire scattering patterns, as they could be described by a model consisting of only unimers and micelles of an aggregation number close to their final value. Thus, the kinetic model is not only consistent with the forward scattering (through p_w), but with the information obtained from the entire q range covered. The polydispersity of the micelles, as shown in Figure 7, cannot be compared to the results from the structural model fit, as the

dx.doi.org/10.1021/ja312469n | J. Am. Chem. Soc. 2013, 135, 7214−7222

structural model did not include polydispersity of the micelles for the reasons given above.

CONCLUSIONS

By rapid mixing of a solution of singly dissolved DDM molecules in DMF with water, we have observed for the first time the structural kinetics underlying the nonisothermal formation of micelles from a reservoir of unimers by synchrotron SAXS. The series of time-resolved scattering data for different surfactant concentrations could be modeled by a mixture consisting of singly dissolved surfactants and nearly formed ellipsoidal micelles.

The results are consistent with a mechanism where the micelles form and grow by stepwise insertion/expulsion of single surfactant molecules. This applies both for the scattered intensities at low q, giving a model independent determination of the weight-average aggregation numbers, and for results obtained for the modeling of the full scattering patterns in terms of singly dissolved surfactants and ellipsoidal micelles. Thus, it is concluded that insertion/expulsion of single surfactant molecules is the dominant mechanism for the equilibration process in surfactant solutions. Fusion/fission of micelles cannot be ruled out; however, the absence of indications for premicellar aggregates with aggregation numbers significantly below that of the final micelles is consistent with the insertion/expulsion mechanism.

In summary, this work provides a detailed insight into the complete process of surfactant micelle formation under nonisothermal conditions. By resolving the structural evolution in real time and describing the kinetics involved, the results presented give highly quantitative information that can be very useful for designing surfactant systems for potential applications. The presented experimental method and modeling approach are also likely to find applications to studies of other physicochemical kinetic processes.

ASSOCIATED CONTENT

Supporting Information

Determination of cmc by surface tension measurements, dynamic light scattering, and SAXS is given together with solvent viscosity measurements for the relevant temperature interval and X-ray scattering contrast determinations from densimetry. Time-resolved SAXS data for all the investigated surfactant concentrations are shown as well as data and model fits for premixed samples. The calculation of the weight-average aggregation number from the scattering data is given. The temporal evolution of the number of unimers and dimers, as resulting from the fit of the kinetic model, is plotted for the lowest and highest investigated surfactant concentration, respectively. This material is available free of charge via the Internet at http://pubs.acs.org.

AUTHOR INFORMATION

Corresponding Author

gvjensen@nbi.ku.dk

Present Addresses

[⊥]Niels Bohr Institute, University of Copenhagen, Universitetsparken 5, DK-2100 Copenhagen, Denmark

[#]Department of Chemistry, University of Oslo, Postbox 1033 Blindern, 0315 Oslo, Norway

Notes

The authors declare no competing financial interest.

ACKNOWLEDGMENTS

We acknowledge the European Synchrotron Radiation Facility for providing access to beamline ID02.

REFERENCES

(1) Buist, I.; Potter, S.; Nedwed, T.; Mullin, J. *Cold Reg. Sci. Tech.* **2011**, *67*, 3.
(2) Haigh, S. D. *Sci. Total Environ.* **1996**, *185*, 161.
(3) Kralova, I.; Sjoblom, J. *J. Dispersion Sci. Technol.* **2009**, *30*, 1363.
(4) Nazar, M. F.; Shah, S. S.; Khosa, M. A. *Pet. Sci. Technol.* **2011**, *29*, 1353.
(5) Nitschke, M.; Costa, S. G. V. A. O. *Trends Food Sci. Technol.* **2007**, *18*, 252.
(6) Pacwa-Plociniczak, M.; Plaza, G. A.; Piotrowska-Seget, Z.; Cameotra, S. S. *Int. J. Mol. Sci.* **2011**, *12*, 633.
(7) Tadros, T.; Izquierdo, P.; Esquena, J.; Solans, C. *Adv. Colloid Interface Sci.* **2004**, *108−109*, 303.
(8) Holmberg, K.; Jönsson, B.; Kronberg, B.; Lindman, B. *Surfactants and Polymers in Aqueous Solution*; Wiley: Hoboken, NJ, 2002.
(9) Giddi, H. S.; Arunagirinathan, M. A.; Bellare, J. R. *Indian J. Exp. Biol.* **2007**, *45*, 133.
(10) Lawrence, M. J. *Chem. Soc. Rev.* **1994**, *23*, 417.
(11) Pouton, C. W. *Eur. J. Pharm. Sci.* **2000**, *11*, S93.
(12) Antonietti, M. *Curr. Opin. Colloid Interface Sci.* **2001**, *6*, 244.
(13) Chern, C. S. *Prog. Polym. Sci.* **2006**, *31*, 443.
(14) Chevalier, Y.; Zemb, T. *Rep. Prog. Phys.* **1990**, *53*, 279.
(15) Dupuy, C.; Auvray, X.; Petipas, C.; Rico-Lattes, I.; Lattes, A. *Langmuir* **1997**, *13*, 3965.
(16) Hoffmann, H.; Ebert, G. *Angew. Chem., Int. Ed. Engl.* **1988**, *27*, 902.
(17) Hayter, J. B.; Penfold, J. *Colloid Polym. Sci.* **1983**, *261*, 1022.
(18) Iampietro, D. J.; Brasher, L. L.; Kaler, E. W.; Stradner, A.; Glatter, O. *J. Phys. Chem. B* **1998**, *102*, 3105.
(19) Penfold, J.; Tucker, I.; Thomas, R. K.; Staples, E.; Schuermann, R. *J. Phys. Chem. B* **2005**, *109*, 10760.
(20) Zana, R. *Adv. Colloid Interface Sci.* **1995**, *57*, 1.
(21) Ericsson, C. A.; Söderman, O.; Garamus, V. M.; Bergström, M.; Ulvenlund, S. *Langmuir* **2005**, *21*, 1507.
(22) Bergström, M.; Pedersen, J. S. *J. Phys. Chem. B* **1999**, *103*, 8502.
(23) Bergström, L. M.; Bastardo, L. A.; Garamus, V. M. *J. Phys. Chem. B* **2005**, *109*, 12387.
(24) Pedersen, J. S. In *Soft Matter Characterization*; Borsali, R., Pecora, R., Eds.; Springer: Netherlands, 2008; p 191.
(25) Patist, A.; Oh, S. G.; Leung, R.; Shah, D. O. *Colloids Surf., A* **2001**, *176*, 3.
(26) Patist, A.; Kanicky, J. R.; Shukla, P. K.; Shah, D. O. *J. Colloid Interface Sci.* **2002**, *245*, 1.
(27) Lang, J.; Tondre, C.; Zana, R.; Bauer, R.; Hoffmann, H.; Ulbricht, W. *J. Phys. Chem.* **1975**, *79*, 276.
(28) Aniansson, E. A. G.; Wall, S. N.; Almgren, M.; Hoffmann, H.; Kielmann, I.; Ulbricht, W.; Zana, R.; Lang, J.; Tondre, C. *J. Phys. Chem.* **1976**, *80*, 905.
(29) Kresheck, G. C.; Hamori, E.; Davenport, G.; Scheraga, H. A. *J. Am. Chem. Soc.* **1966**, *88*, 246.
(30) Bennion, B. C.; Eyring, E. M. *J. Colloid Interface Sci.* **1970**, *32*, 286.
(31) Muller, N. *J. Phys. Chem.* **1972**, *76*, 3017.
(32) Tondre, C.; Zana, R. *J. Colloid Interface Sci.* **1978**, *66*, 544.
(33) Tondre, C.; Lang, J.; Zana, R. *J. Colloid Interface Sci.* **1975**, *52*, 372.
(34) Takeda, K.; Yasunaga, T. *J. Colloid Interface Sci.* **1972**, *40*, 127.
(35) Lessner, E.; Teubner, M.; Kahlweit, M. *J. Phys. Chem.* **1981**, *85*, 3167.
(36) Lessner, E.; Teubner, M.; Kahlweit, M. *J. Phys. Chem.* **1981**, *85*, 1529.
(37) Jaycock, M.; Ottewill, R. H. Proceedings of 4th International Congress on Surface Active Substances Brussels, Brussels, Belgium,

September 7−12, 1964; Gordon and Breach Science Publishers: London, 1964; p 8.
(38) Rharbi, Y.; Winnik, M. A. *J. Phys. Chem. B* **2003**, *107*, 1491.
(39) Zhang, J.; Ge, Z.; Jiang, X.; Hassan, P. A.; Liu, S. *J. Colloid Interface Sci.* **2007**, *316*, 796.
(40) Zhang, J.; Liu, S. *Phys. Chem. Chem. Phys.* **2011**, *13*, 12545.
(41) Bryskhe, K.; Bulut, S.; Olsson, U. *J. Phys. Chem. B* **2005**, *109*, 9265.
(42) Eastoe, J.; Dalton, J. S.; Downer, A.; Jones, G.; Clarke, D. *Langmuir* **1998**, *14*, 1937.
(43) Aniansson, E. A. G.; Wall, S. N. *The Journal of Physical Chemistry* **1974**, *78*, 1024.
(44) Aniansson, E. A. G.; Wall, S. N. *The Journal of Physical Chemistry* **1975**, *79*, 857.
(45) Kahlweit, M. *J. Colloid Interface Sci.* **1982**, *90*, 92.
(46) Lund, R.; Willner, L.; Monkenbusch, M.; Panine, P.; Narayanan, T.; Colmenero, J.; Richter, D. *Phys. Rev. Lett.* **2009**, *102*, 188301.
(47) Neu, J. C.; Cañizo, J. A.; Bonilla, L. L. *Phys. Rev. E* **2002**, *66*, 061406.
(48) Nyrkova, I. A.; Semenov, A. N. *Macromol. Theory Simul.* **2005**, *14*, 569.
(49) Mohan, G.; Kopelevich, D. I. *J. Chem. Phys.* **2008**, *128*, 044905.
(50) Gottberg, F. K. v.; Smith, K. A.; Hatton, T. A. *J. Chem. Phys.* **1998**, *108*, 2232.
(51) Kegeles, G. *J. Phys. Chem.* **1979**, *83*, 1728.
(52) Narayanan, T. *Curr. Opin. Colloid Interface Sci.* **2009**, *14*, 409.
(53) Egelhaaf, S. U. *Curr. Opin. Colloid Interface Sci.* **1998**, *3*, 608.
(54) Panine, P.; Finet, S.; Weiss, T. M.; Narayanan, T. *Adv. Colloid Interface Sci.* **2006**, *127*, 9.
(55) Gradzielski, M. *Curr. Opin. Colloid Interface Sci.* **2004**, *9*, 256.
(56) Schmölzer, S.; Gräbner, D.; Gradzielski, M.; Narayanan, T. *Phys. Rev. Lett.* **2002**, *88*, 258301.
(57) Gradzielski, M. *Curr. Opin. Colloid Interface Sci.* **2003**, *8*, 337.
(58) Weiss, T. M.; Narayanan, T.; Wolf, C.; Gradzielski, M.; Panine, P.; Finet, S.; Helsby, W. I. *Phys. Rev. Lett.* **2005**, *94*, 038303.
(59) Weiss, T. M.; Narayanan, T.; Gradzielski, M. *Langmuir* **2008**, *24*, 3759.
(60) Egelhaaf, S. U.; Schurtenberger, P. *Phys. B (Amsterdam, Neth.)* **1997**, *234−236*, 276.
(61) Egelhaaf, S. U.; Schurtenberger, P. *Phys. Rev. Lett.* **1999**, *82*, 2804.
(62) Leng, J.; Egelhaaf, S. U.; Cates, M. E. *Biophys. J.* **2003**, *85*, 1624.
(63) Egorov, G.; Kolker, A. *Russ. J. Phys. Chem. A* **2008**, *82*, 2058.
(64) Ueno, M.; Mitsui, R.; Iwahashi, H.; Tsuchihashi, N.; Ibuki, K. *J. Phys.: Conf. Ser.* **2010**, *215*, 012074.
(65) Vass, S.; Torok, T.; Jakli, G.; Berecz, E. *J. Phys. Chem.* **1989**, *93*, 6553.
(66) Guinier, A. *Ann. Phys. (Paris)* **1939**, *12*, 161.
(67) Halperin, A. *Macromolecules* **1987**, *20*, 2943.
(68) Hadgiivanova, R.; Diamant, H.; Andelman, D. *J. Phys. Chem. B* **2010**, *115*, 7268.
(69) Smoluchowski, Z. *Phys. Chem.* **1917**, *92*, 129.
(70) Griffiths, I.; Bain, C.; Breward, C.; Chapman, S.; Howell, P.; Waters, S. *SIAM J. Appl. Math.* **2012**, *72*, 201.